Biomedical Engineering Letters (2022) 12:125–133
https://doi.org/10.1007/s13534-022-00224-0

REVIEW ARTICLE

Slit-based photoacoustic tomography with co-planar light illumination and acoustic detection for high-resolution vascular imaging in human using a linear transducer array

Wenhan Zheng[1] · Chuqin Huang[1] · Huijuan Zhang[1] · Jun Xia[1]

Received: 24 December 2021 / Revised: 18 February 2022 / Accepted: 25 February 2022 / Published online: 26 March 2022

Abstract
Slit-based photoacoustic tomography is a high-resolution three-dimensional imaging technique for linear transducer array. The system was based on acoustic diffraction through a thin slit to increase the elevation coverage and spatial resolution. In this study, we introduce the third-generation slit-based photoacoustic tomography system with co-planar light illumination and acoustic detection. The new system possesses several innovations. First, we utilized an optically transparent slit, which enables both light illumination and acoustic diffraction. Second, we used a combination of cold and hot mirrors to provide co-planar light illumination and acoustic detection. Third, we designed a waterproof transducer array with a long acoustic focus tailored for the co-planar setup. Compared to the previous generations, which used side-illumination and metal slit, the new system provides a larger field of view and deeper imaging depth in a more compact manner. We tested the system in both phantoms and in vivo imaging. Detailed vascular structures from different regions can be clearly revealed, making the system valuable for translational imaging applications.

Keywords Photoacoustic tomography · Resolution enhancement · Linear transducer array · Vascular imaging · Three-dimensional imaging

1 Introduction

Capitalizing on the photoacoustic effect, photoacoustic tomography (PAT) offers deep tissue imaging of optical contrasts at a high spatial resolution [1, 2]. Over the past few years, PAT is becoming a competitive imaging modality for biomedical research and preclinical imaging. Linear-array-based transducers have been widely used in PAT due to their high compatibility with existing ultrasound systems and low cost [3, 4]. However, the resolving power of a linear array along the elevation direction is poor compared to that of axial and lateral directions. Therefore, linear arrays are not well suited for three-dimensional imaging. Various approaches have been proposed to address this issue through adjusting the scanning geometries or developing advanced image reconstruction techniques [5, 6]. Previously, we discovered that the acoustic diffraction effect could be utilized to improve the receiving angle of the transducer. This discovery led to the development of the first generation slit-PAT system. In that system, a thin slit was placed along the elevation focus of the linear array. The slit allowed acoustic waves coming out of the elevation focal zone to be effectively detected, enlarging the elevation coverage and improving the resolution [7]. Our first-generation slit-based system achieved nearly isotropic spatial resolution in all three dimensions. However, in that system, the transducer and light source remained stationary and the object needed to be rotated inside a water bath, impeding the implementation for in vivo imaging. Later, we proposed the second generation slit-PAT system, consisting of a more compact scanning head that could scan across an object [8]. In addition, the slit width can be adjusted based on the imaging needs. For instance, the slit width can be reduced when a higher resolution image is needed, and the width can be enlarged when a better signal-to-noise ratio (SNR) is desired [9, 10]. However, due to the utilization of side illumination, the second slit-PAT is still relatively bulky, and the imaging depth is heavily dependent on the light incident angle [11, 12].

✉ Jun Xia
junxia@buffalo.edu

[1] Department of Biomedical Engineering, University at Buffalo North Campus, Buffalo, NY 14260, USA

To overcome these limitations, we introduce the third generation slit-PAT with improvement in three aspects. First, the slit is now formed by borosilicate cover glasses instead of metal blades. The cover glass is optically transparent and facilitates the light illumination design. Second, we used a light-acoustic combiner to achieve co-planar light illumination and acoustic detection, which is essential for deep-tissue imaging [13]. In addition, in our co-planar design, the transducer and fiber bundle are parallel, improving the compactness of the scanning head. Third, as the co-planar design increases the distance of acoustic wave propagation, we custom-designed a transducer array with a longer acoustic focus and lateral length. The transducer is also waterproof and has a cubic shape for easy mounting with the optical fiber bundle. These improvements allow deeper tissue imaging and a larger field of view compared to previous slit-PAT systems. The performance of the new system was tested through various phantom and human imaging studies.

2 Methods

2.1 System design

Figure 1a shows a schematic drawing of the slit-based PAT system. The PAT system consists of the custom-made linear transducer array, a data acquisition system (DAQ), and a Q-switched Nd:YAG laser. The linear transducer array (L5), made by Imasonic, has 128 elements and a lateral length of 50 mm. The central frequency and the focal length are 5 MHz (bandwidth $\geq 65\%$ at -6 dB) and 40 mm, respectively. Each element has a size of 0.4 by 15 mm. Light illumination is provided by a Surelite SL III – 10 laser (Continuum) with 1064 nm output wavelength, < 10 ns pulse width, and 10 Hz pulse repetition frequency. The maximum output power is 8 W. Acoustic data is acquired by a 256-channel data acquisition unit (Vantage-256, Verasonic Inc.).The transducer is mounted on a lab-made holder, which combines the transducer and the fiber bundle. The holder also enables co-planar light illumination and acoustic detection. As shown in Fig. 1a, a cylindrical lens is mounted at the end of the fiber output to collimate the diffused fiber output. A

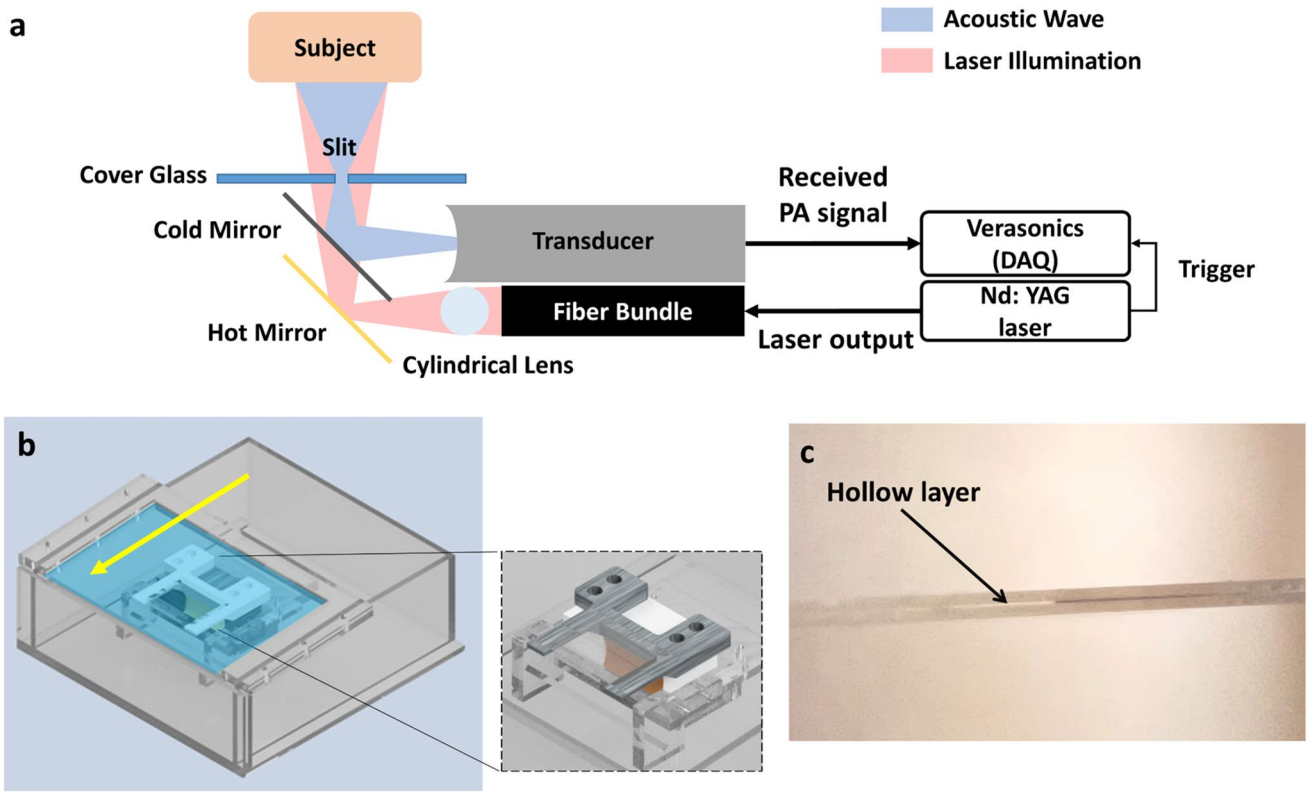

Fig. 1 Experimental setup of the slit-based system. **a** Schematic drawing of system setup. Blue and red represent the acoustic wave and laser beam, respectively. **b** 3D drawing of the scanning head placed inside the watertank. The yellow arrow represents the scanning direction. The blue transparent area represents the polyester film mounted on the top opening. A zoom-in view of the scanning head is shown in the dashed box. **c** A photograph of the glued two-layer glass

high-performance hot mirror (> 95% reflection at 1064 nm, Edmund Optics Inc.) is placed in front of the fiber output to reflect the light by 90 degrees. The reflected light will pass through a cold mirror, which has over 90% transmission at 1064 nm (High-performance cold mirror, Edmund Optics Inc.). The light will then go through the cover-glass-formed slit to reach the object. The size of light beam on human skin is approximately 20 by 50 mm. The generated photoacoustic waves will be reflected by the cold mirror before reaching the transducer. This design significantly improved the light illumination efficiency. In comparison, the first and second-generation systems used side light illumination. Before imaging, the scanning head will be placed in a water tank filled with deionized water. The water tank has an opening at the top sealed with 0.001″-thick polyester film, which serves as the imaging window (Fig. 1b). Scanning is performed by a motorized translation stage (MSS33-150065, Thomsom Industries, Inc.) and controlled by a function generator (SDG2042X, SIGLENT). The slit is formed by two microscope cover glasses (0330-4050, Kemtech America, Inc.) with a dimension of 24 mm × 60 mm and thicknesses ranging from 0.13 to 0.16 mm. When thicker cover glasses were needed, we glued two cover glasses with Loctite super glue. The glue was applied to the edges of the glass, leaving air in the center for good acoustic signal rejection (Fig. 1c). At zero-degree incident angle, we verified that 90% of 1064 nm light could pass through the glued cover glass. Two sets of cover glasses are installed on a customized holder to form the slit, and the slit width is adjustable. Compared to the first and second-generation designs where opaque metal blades were used, the cover glass is optically transparent (90% transparency with 1064 nm input), allowing it to be integrated into the double-mirror design. Table 1 summarizes the main differences between different slit-PAT systems.

2.2 Experimental procedure

For all experiments, the object is placed on the membrane at the top of the water tank. Ultrasound gel (PARKER laboratories Inc.) is used to improve coupling between the plastic membrane and the object. The scanning head moves horizontally along the elevation direction of the transducer (yellow arrow in Fig. 1a) at a speed of 1 mm/s. The overall scanning range is 50 mm, and the final field of view is 50 mm by 50 mm (lateral length of the transducer). The total scanning time is 50 s. Two phantom experiments were performed to quantify the system performance. The first was a cross-line phantom, where two 0.1 mm-width lines are printed on a transparent film (Fig. 2a). The second phantom was made by pencil leads. As shown in Fig. 2b, four 0.2 mm pencil leads were embedded in an agar phantom. Spacing between pencil leads is 1 cm, and they are arranged at 45-degree angle to the horizontal plane. The human imaging study was performed on the palm and forearm of healthy human subjects. The

Table 1 Comparison of first, second, and third-generation slit PAT systems

	Illumination	Slit material	Slit width (mm)	Transducer
First-generation	Stationary side illumination	Iron material	0.3	Philips L7-4
Second-generation	Side illumination	316 Stainless Steel	0.6*	Philips L7-4
Third-generation	Co-planar with acoustic detection	Borosilicate cover glass	0.6*	Imasonic L5

The slit widths in the second and third generations are adjustable (marked with *)

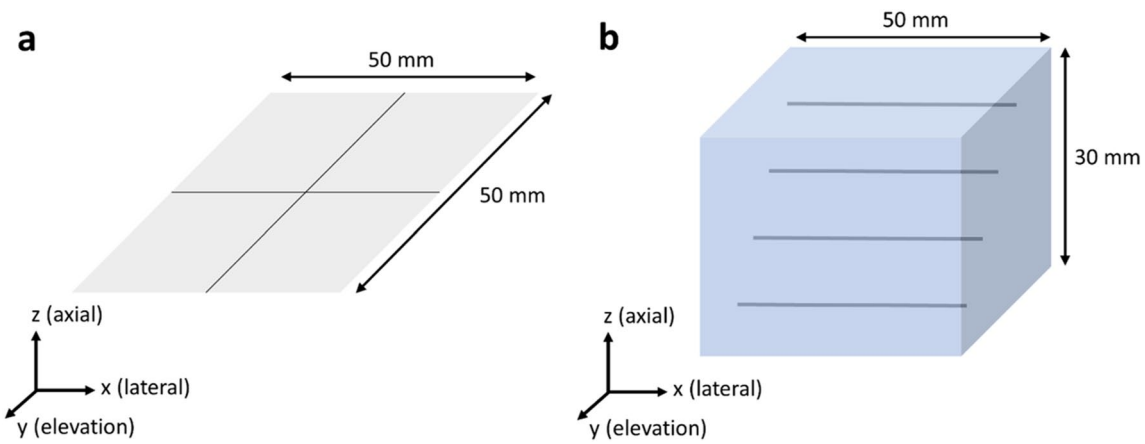

Fig. 2 Schematic drawing of test phantoms. **a** Cross-line phantom. **b** Pencil lead phantom

study has been reviewed and approved by the University at Buffalo Institutional Review Board (IRB). Informed consent was obtained from all individual participants included in the study. All experiments were performed in accordance with relevant guidelines and regulations. The input laser intensity on the skin surface was estimated to be around 38 mJ/cm^2, which is below the 100 mJ/cm^2 limit defined by the American National Standards Institute (ANSI) [14].

2.3 Reconstruction

Two reconstruction methods could be used in the study. The first is 2D reconstruction and stack (2D-Stack). In this method, each image frame is reconstructed independently. All frames are then stacked according to their positions in the 3D scan. This reconstruction method is fast (< 20 s) and suitable for quick visualization of the experimental result. The second method is 3D reconstruction. In this method, the time-of-arrival in the 3D domain was considered in the reconstruction. When there is no slit, we used the focal line of the linear transducer array as a guideline to calculate the arrival time. When the slit is present, we use the slit position as the guideline for calculation. This method was named 3D-focal-line (3DFL) image reconstruction, and more details can be found in references [15, 16]. Because each frame was reconstructed using data from all acquisition positions, 3DFL reconstruction takes longer (10 min in a 2080Ti GPU) than the 2D-stack method, but it renders a more accurate (higher resolution) result [17]. Therefore, all data presented in this study were reconstructed using 3DFL. After reconstruction, the 3D image is displayed with depth-encoded maximum intensity projection (MIP).

3 Results

We first quantified the resolution based on the full width at half maximum (FWHM) along lateral and elevation directions of the cross-line phantom. Our previous study indicates that the elevation resolution becomes larger while the slit width increases [8]. In the meanwhile, PA signal intensity increases as more acoustic energy pass through the slit. We quantified the resolution along lateral and elevation directions for different slit widths. As expected, the slit width has little impact on the lateral resolution, while the elevation resolution gradually improves while the slit width increases. An exception is at the 0.3-mm slit width, where both lateral and elevation resolutions are significantly worse than those at larger slit widths. We believe that could be caused by acoustic oscillation within the slit, because the slit width is comparable to the slit thickness. To reduce this effect, we used a single layer of cover glass (0.16 mm) to form the 0.3 mm slit. However, the single layer cannot provide sufficient signal rejection due to the missing hollow layer. Hence, the received PA signals were combined with the transmitted and diffracted acoustic waves, reducing the resolution of the reconstructed image. As can be seen in Table 2, when a thinner slit is applied, the quantified resolution is still worse than that of the 0.6 mm slit width. Therefore, all future experiments were performed with a 0.6 mm slit width. Figure 3a, b show the reconstructed cross-line phantom image without and with the 0.6-mm slit, respectively. In a separate experiment, we also quantified the axial resolution of our system using the finest cross-section of the vessel from the in vivo image. The axial resolution of the image with 0.6 mm slit width and without slit is quantified to be 0.38 mm and 0.37 mm, respectively.

We also quantified the elevation resolution at different depths by scanning the pencil lead phantom mentioned in the method section (Fig. 2b). Results are shown in Fig. 4. Figure 4a, b show raw-channel data acquired by element 64, without and with the use of slit, respectively. As can be seen in Fig. 4a, due to the limited receiving angle, pencil lead signals rapidly decreased while the subject was out of the focal zone of the transducer (marked by yellow dashed lines). With the use of slit, the detected PA signals were captured over a larger scanning distance compared to the signals without slit, which means the receiving angle of the transducer is improved (Fig. 4b). The 3DFL reconstruction results acquired without and with slit are displayed in Fig. 4c, d, respectively. The color scales in both images represent distance to the transducer. Compared to the one without slit, the image with slit exhibits a finer elevation resolution at different imaging depths. These results demonstrate that our system provides improved resolution for objects located far away from the transducer.

In vivo experiments.

Table 2 System performance quantification

Slit width (mm)	0.3 (single layer)	0.3 (double layer)	0.6 (double layer)	0.9 (double layer)	1.2 (double layer)	No slit
Lateral resolution (mm)	0.66	0.48	0.41	0.43	0.43	0.42
Elevation resolution (mm)	0.57	1.18	0.35	0.40	0.54	1.30
Signal intensity (a.u.)[a]	0.9	1.0	1.9	2.3	2.3	3.1

[a]Mean intensity of the object in the non-normalized reconstructed image

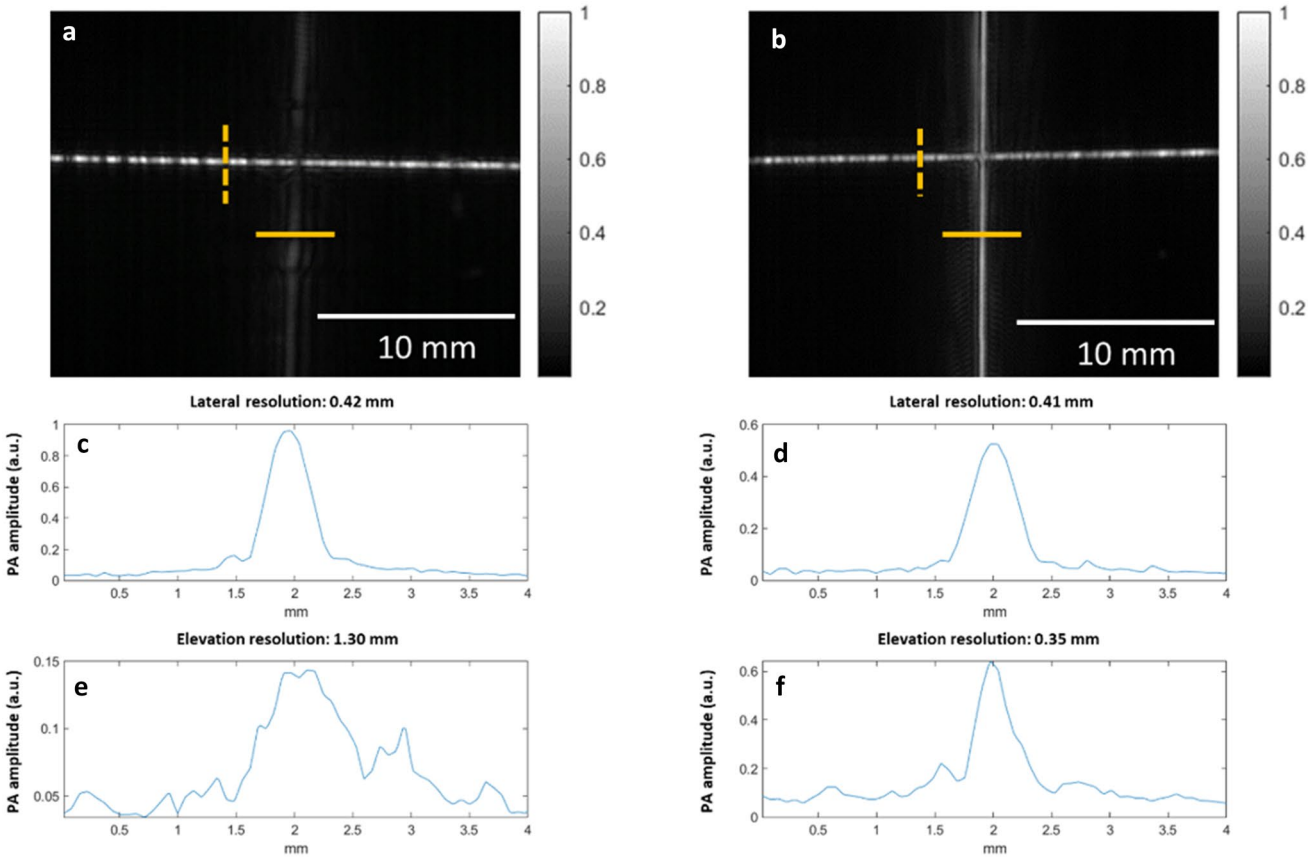

Fig. 3 Maximum amplitude projection of the cross-line phantom images acquired **a** without and **b** with the use of slit. **c** Lateral resolution quantified by PA signal intensity along the dashed yellow line in **a**. **d** Lateral resolution quantified by PA signal intensity along the dashed yellow line in **b**. **e** Elevation resolution quantified by PA signal intensity along the solid yellow line in **a**. **f** Elevation resolution quantified by PA signal intensity along the solid yellow line in **b**

Following the phantom experiment, we imaged the palm and forearm of human subjects to demonstrate the in vivo imaging capability. Vascular images acquired without (left) and with (right) slit are shown in Fig. 5, respectively. The reconstruction depth for palm results was 10 mm, while the depth for the forearm results was 15 mm. The depth-encoded image acquired with slit clearly revealed detailed vascular features. In particular, vessels parallel to the lateral direction exhibit finer structures due to the improved elevation resolution. In the meanwhile, the ones parallel to the elevation direction remain the same sharpness, and the overall vessel continuity is improved especially at the branching points. For better illustration, we used arrows with the same number to mark the same structures located in the middle and right images. Due to the improved elevation resolution, the slit-based system can better reveal small vessels (such as vessels marked by arrow 1 in the first row and arrow 2 in the second row). Moreover, arteries beneath the venous network can be clearly captured in both palm images, benefiting from the improved resolution (such as vessels marked by arrow 4 in the first and second rows).

4 Discussion

We developed the third-generation slit-PAT system with better light illumination schemes and improved compactness. Our custom-made transducer also possesses a larger field of view and better sensitivity than the ones used in previous slit-PAT systems. The transducer (Philips L7-4) utilized in the first and second-generation slit PAT systems was designed for handheld ultrasound. An acoustic lens was mounted in front of the transducer elements. The sensitivity of the transducer is decreased due to the impedance mismatch between elements and lens. Moreover, the focal length of the transducer is too short for the double-mirror design, where the acoustic wave propagation distance is increased. In comparison, the custom-designed transducer possesses a larger transducer element size and longer acoustic focus, and utilizes curved elements for focusing. These designs improve the sensitivity of our system and enable co-planar light illumination and acoustic detection. Compared to results acquired by the first and second-generation slit PAT systems, we found that the images captured by our proposed

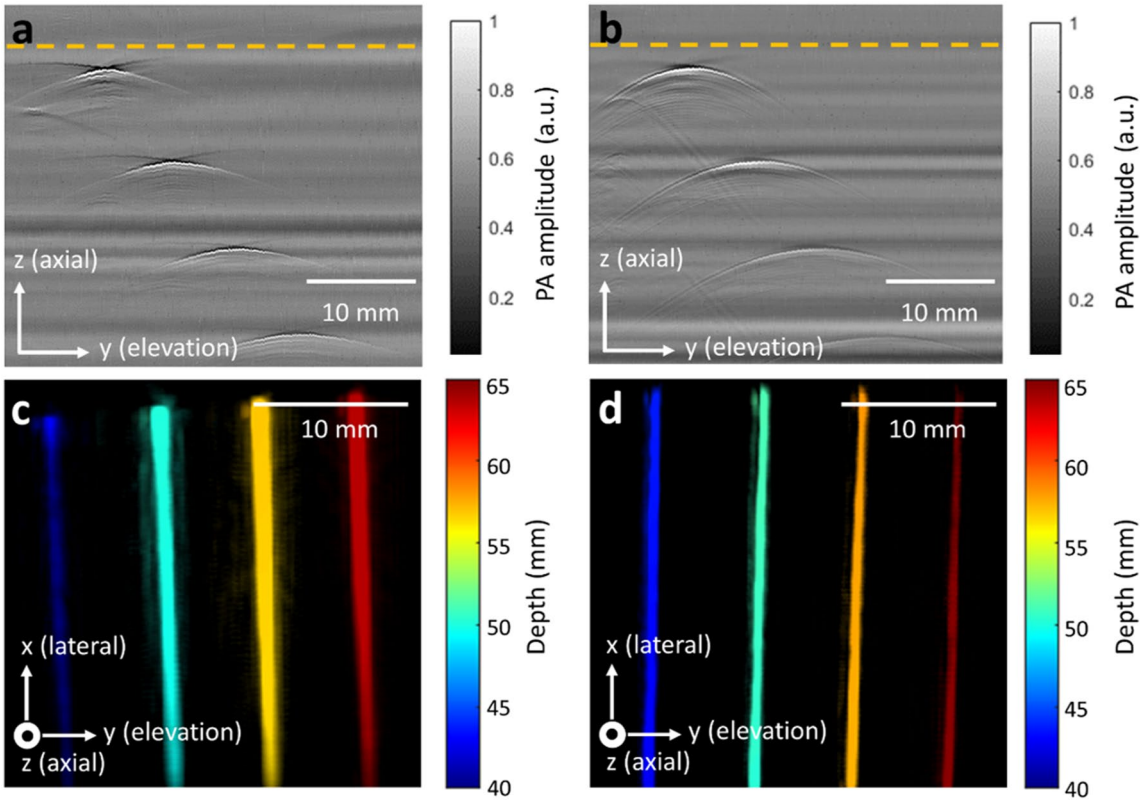

Fig. 4 The raw data and reconstruction results of the pencil-lead phantom. **a** Element 64 raw data presented in the axial and elevation plane (acquired without slit). The transducer's focal region is marked with a yellow dashed line. **b** Element 64 raw data presented in the axial and elevation plane (with slit). The transducer's focal region is marked with a yellow dashed line. **c** Depth-encoded 3D reconstructed image acquired without slit. **d** Depth-encoded 3D reconstructed image acquired with slit

system exhibited deeper imaging depth. For instance, in the palm result, the arteries can be clearly revealed in Fig. 5c, while it was invisible in the Gen 2 slit PAT system [8]. A detailed analysis of the arm result can be found in Fig. 6, where the Gen 3 and Gen 2 results are plotted side by side. It can be seen clearly that the new system provided deeper imaging depth and a larger field of view.

To quantify the amount of acoustic energy reflected by the cover glass, we simulated the acoustic propagation using MATLAB-based K-wave toolbox [18] in three conditions: without the slit, with a single layer of cover glass, and with two layers of glass. As shown in Fig. 7a, an arc-shaped transducer was created to represent one element in the L5 transducer. The glass layer is placed 40 mm underneath the transducer and a point source was created underneath the glass to represent a point optical absorber. The acoustic properties of the glass are defined according to the reference [19]. Figure 7b shows the received A-line signal in three conditions. The blue A-line represents the received signal without the glass layer. The red A-line denotes the received signal after applying a single layer of glass. Compared to the signal without glass, the peak PA amplitude decreases by about 70 percent. The black A-line represents the received signal after applying a double glass layer with a hollow layer in between. The transmitted acoustic signal is negligible. According to these simulation results, we can conclude that a single layer of glass cannot provide sufficient acoustic signal rejection. That is probably why the single layer results in Table 2 are poorer than the others.

While the proposed system exhibits improved compactness and elevation resolution, it can be further improved for better vascular imaging. For instance, the slit installation and width adjustment are time-consuming, as the slit is manually mounted on the holder, and the width needs to be calibrated after mounting. This issue can be addressed by utilizing a micrometer-adjustable slit holder. Moreover, the DAQ has an internal jittering which creates a small shift among frames (seen as discontinuity in vessels). In the future, an external trigger can be applied to our system to allow precise synchronization of data acquisition and laser firing. Another issue is the relatively slow scanning speed, which is susceptible to body motion. A higher imaging speed could be achieved using a higher pulse repetition rate laser. For instance, using a 500 Hz laser, we could image the whole palm in 1 s.

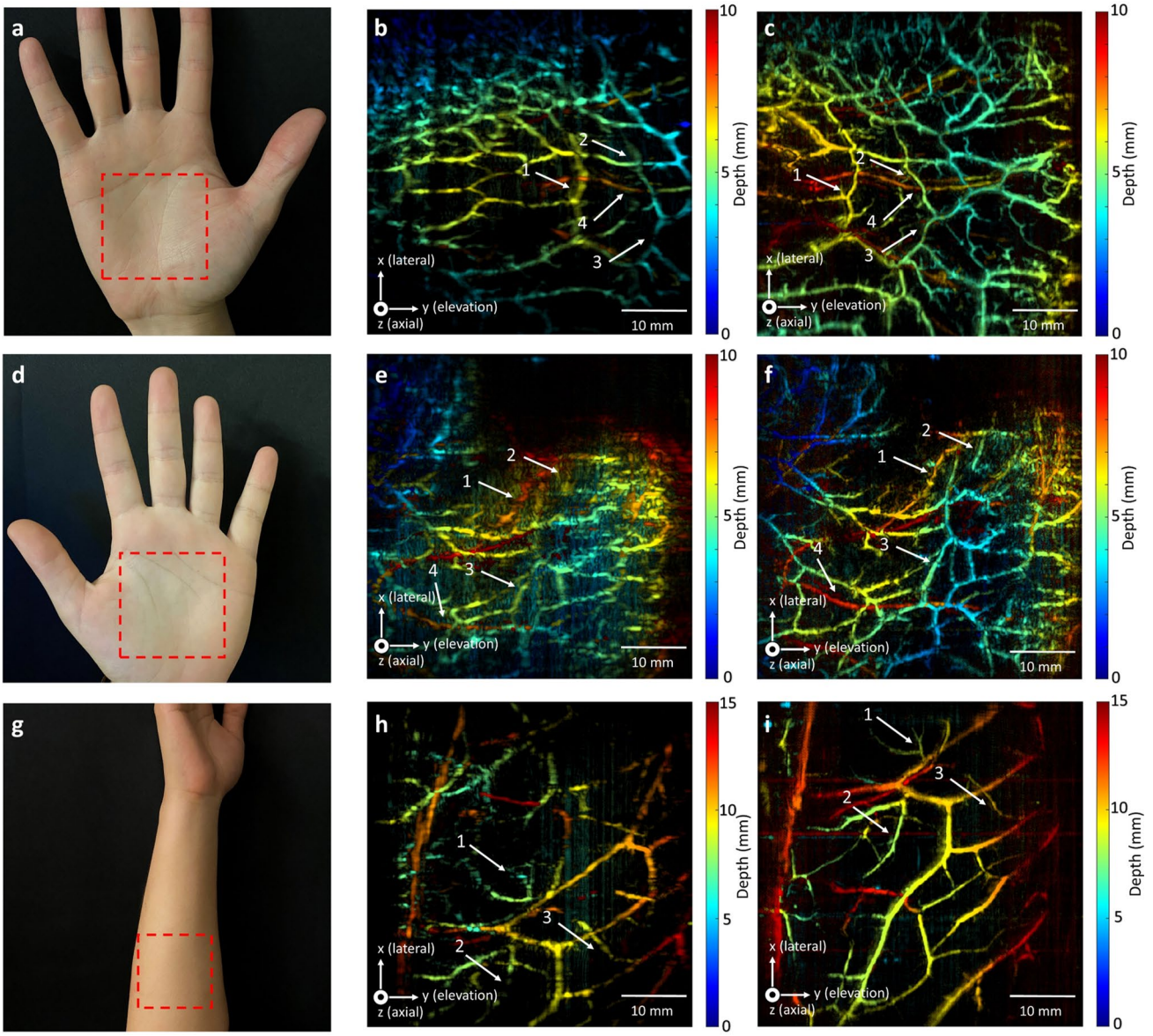

Fig. 5 In vivo experiments performed without and with the slit. **a** A photograph of the palm of volunteer 1. **b** Depth-encoded palm vascular image of volunteer 1 acquired without slit. **c** Depth-encoded palm vascular image of volunteer 1 acquired with slit. **d** A photograph of the palm of volunteer 2. **e** Depth-encoded palm vascular image of volunteer 2 acquired without slit. **f** Depth-encoded palm vascular image of volunteer 2 acquired with slit. **g** A photograph of the forearm of volunteer 3. **h** Depth-encoded forearm vascular image of volunteer 3 acquired without slit. **i** Depth-encoded forearm vascular image of volunteer 3 acquired with slit. The numbered arrows mark the same vessels in the middle and right column of images

5 Conclusion

This study demonstrated the third generation slit-PAT system with co-planar light illumination and acoustic detection using an optically transparent slit and a double mirror setup. A customized waterproof transducer with a 40 mm focal length was utilized to better align with the fiber bundle and the double mirror setup. We investigated the effect induced by different cover glass thicknesses and slit widths to optimize the system performance. We found that the double glass layer with 0.6 mm slit width performed the best. We scanned two types of phantoms to quantify the system resolution and demonstrated that our system possesses high elevation resolution at different imaging depths. High-resolution vascular images of the human palm and forearm were also acquired, and the results revealed deeper vessels compared to the ones acquired in previous slit-PAT systems. We envision that slit-PAT will be applied to various vascular imaging applications.

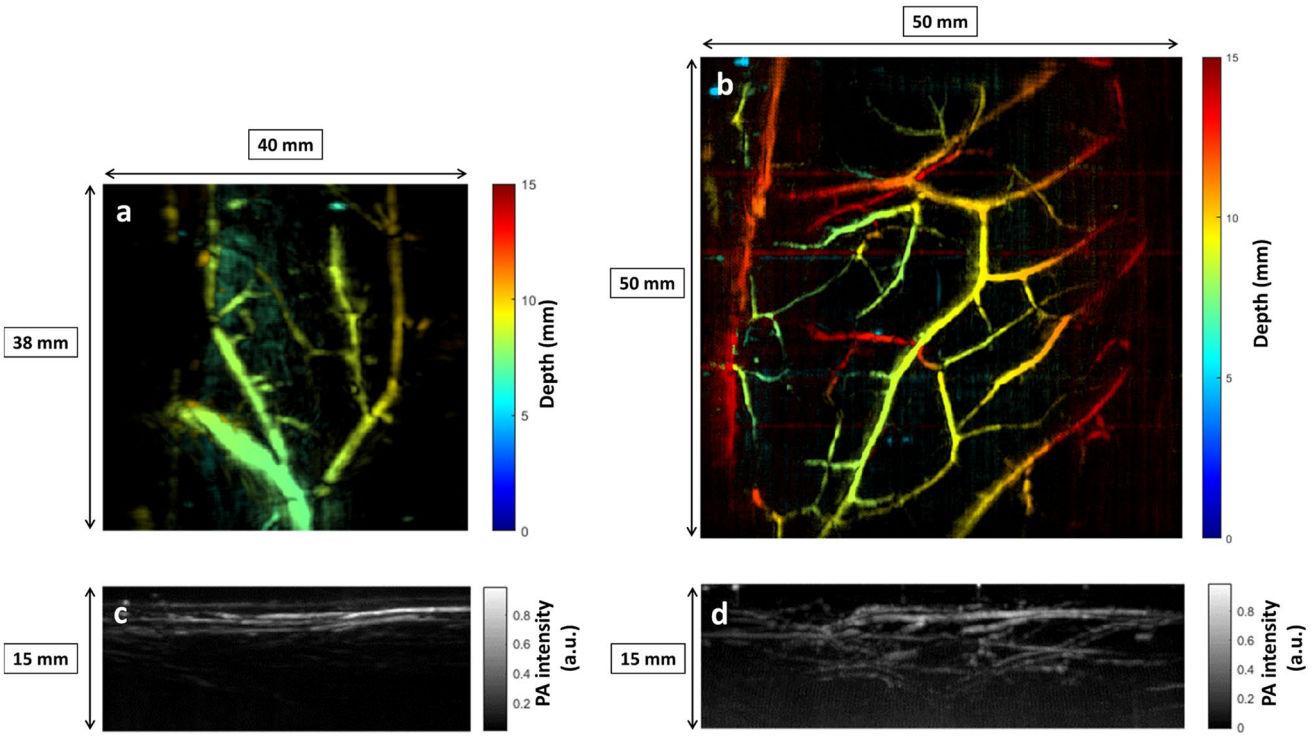

Fig. 6 Comparison of reconstructed image acquired by second and third generation system. **a** Depth-encoded arm vascular image acquired by the second generation system. **b** Depth-encoded arm vascular image acquired by the third generation system. **c** Cross-sectional maximum intensity projection of **a**. **d** Cross-sectional maximum intensity projection of **b**

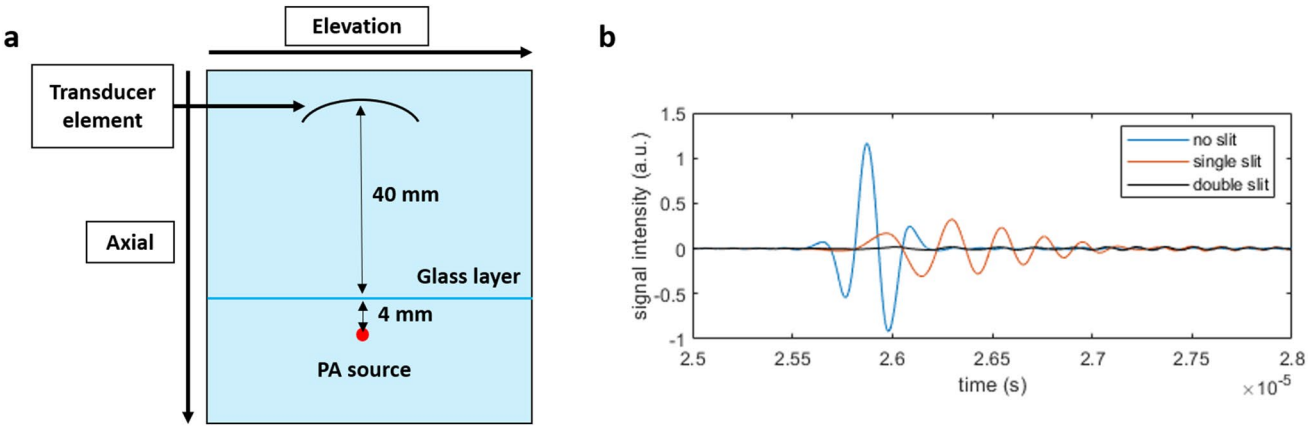

Fig. 7 Simulation results in different conditions. **a** A schematic drawing of the K-wave simulation environment. **b** A-line signals acquired at different conditions

Author contributions JX and WZ conveived and designed the study. WZ and CH constructed the hardware system. WZ and HZ performed the data collection and analysis. JX, WZ, and CH wrote the manuscript and all authors helped with revision. All authors read and approved the final manuscript.

Funding This work was supported by the National Institute of Health under Grants R01EB029596 and R01EB028978.

Declarations

Conflict of interest Dr. Jun Xia is the founder of Sonioptix, LLC, which, however, did not support this work. All other authors declare no conflicts of interest.

Ethical approval All procedures performed in studies involving human participants were in accordance with the ethical standards of the institutional and/or national research committee and with the 1964 Helsinki declaration and its later amendments or comparable ethical standards.

References

1. Xia J, Yao J, Wang LV. Photoacoustic tomography: principles and advances. Electromagn Waves. 2014;147:1–22.
2. Xia J, Wang LV. Small-animal whole-body photoacoustic tomography: a review. IEEE Trans Biomed Eng. 2014;61(5):1380–9.
3. Li G, et al. Multiview Hilbert transformation for full-view photoacoustic computed tomography using a linear array. J Biomed Opt. 2015;20(6):066010.
4. Gateau J, et al. Three-dimensional optoacoustic tomography using a conventional ultrasound linear detector array: whole-body tomographic system for small animals. Med Phys. 2013;40(1):013302.
5. Gateau J, et al. Single-side access, isotropic resolution, and multispectral three-dimensional photoacoustic imaging with rotate-translate scanning of ultrasonic detector array. J Biomed Opt. 2015;20(5):056004.
6. Schwarz M, Buehler A, Ntziachristos V. Isotropic high resolution optoacoustic imaging with linear detector arrays in bi-directional scanning. J Biophotonics. 2015;8(1–2):60–70.
7. Wang Y, et al. Slit-enabled linear-array photoacoustic tomography with near isotropic spatial resolution in three dimensions. Opt Lett. 2016;41(1):127–30.
8. Wang Y, et al. Second generation slit-based photoacoustic tomography system for vascular imaging in human. J Biophotonics. 2017;10(6–7):799–804.
9. Zheng W, Lee D, Xia J. Photoacoustic tomography of fingerprint and underlying vasculature for improved biometric identification. Sci Rep. 2021;11(1):1–9.
10. Zhan Y, et al. 3D finger vein biometric authentication with photoacoustic tomography. Appl Opt. 2020;59(28):8751–8.
11. Wang G, et al. Simulation of light delivery for photoacoustic breast imaging using the handheld probe. Chin Opt Lett. 2014;12(5):51–703.
12. Sivasubramanian K, et al. Optimizing light delivery through fiber bundle in photoacoustic imaging with clinical ultrasound system: Monte Carlo simulation and experimental validation. J Biomed Opt. 2016;22(4):041008.
13. Wang Y, et al. Optimizing the light delivery of linear-array-based photoacoustic systems by double acoustic reflectors. Sci Rep. 2018;8(1):1–7.
14. Institute, A., American National Standard for Safe Use of Lasers. 2007.
15. Xia J, et al. Three-dimensional photoacoustic tomography based on the focal-line concept. J Biomed Opt. 2011;16(9):090505.
16. Wang D, et al. Coherent-weighted three-dimensional image reconstruction in linear-array-based photoacoustic tomography. Biomed Opt Express. 2016;7(5):1957–65.
17. Nyayapathi N, et al. Dual scan mammoscope (DSM)—a new portable photoacoustic breast imaging system with scanning in craniocaudal plane. IEEE Trans Biomed Eng. 2019;67(5):1321–7.
18. Treeby BE, Cox BT. k-Wave: MATLAB toolbox for the simulation and reconstruction of photoacoustic wave fields. J Biomed Opt. 2010;15(2):21314.
19. Conesa J, et al. Geographical and fingerprinting data to create systems for indoor positioning and indoor/outdoor navigation. Elsevier; 2018.